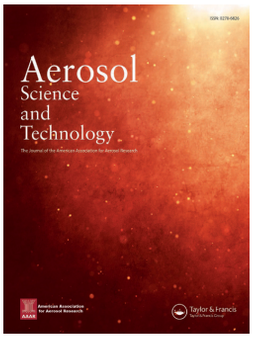

Aerosol Science and Technology

ISSN: 0278-6826 (Print) 1521-7388 (Online) Journal homepage: https://www.tandfonline.com/loi/uast20

Modulation of silica layer properties by varying the granulometric state of tetraethyl orthosilicate precursor aerosols during combustion chemical vapor deposition (CCVD)

Björn Sten Mark Kretzschmar, Paul Bergelt, Daniel Göhler, Fabian Firmbach, Ronny Köcher, Andreas Heft, Michael Stintz & Bernd Grünler

To cite this article: Björn Sten Mark Kretzschmar, Paul Bergelt, Daniel Göhler, Fabian Firmbach, Ronny Köcher, Andreas Heft, Michael Stintz & Bernd Grünler (2020): Modulation of silica layer properties by varying the granulometric state of tetraethyl orthosilicate precursor aerosols during combustion chemical vapor deposition (CCVD), Aerosol Science and Technology, DOI: 10.1080/02786826.2020.1762845

To link to this article: https://doi.org/10.1080/02786826.2020.1762845

Accepted author version posted online: 30 Apr 2020.
Published online: 20 May 2020.

AEROSOL SCIENCE AND TECHNOLOGY
https://doi.org/10.1080/02786826.2020.1762845

Modulation of silica layer properties by varying the granulometric state of tetraethyl orthosilicate precursor aerosols during combustion chemical vapor deposition (CCVD)

Björn Sten Mark Kretzschmar[a], Paul Bergelt[b], Daniel Göhler[b,c], Fabian Firmbach[a], Ronny Köcher[a], Andreas Heft[a], Michael Stintz[b], and Bernd Grünler[a]

[a]Innovent e.V, Jena, Germany; [b]Research Group Mechanical Process Engineering, Institute of Process Engineering and Environmental Technology, Technische Universität Dresden, Dresden, Germany; [c]Topas GmbH, Dresden, Germany

ABSTRACT

For the purpose of silica surface layer modulation, a pneumatic-controlled two-substance atomizer with inertia-based coarse droplet separation was operated at different system pressures for tetraethyl orthosilicate precursor aerosol supply during combustion chemical vapor deposition. A comprehensive testing study was performed to characterize the atomizer's performance characteristics, initial precursor aerosols at the atomizer's outlet, transformed aerosols before combustion, combustion aerosols and formed layers. Laser diffraction spectrometry, differential electrical mobility analyses and condensation particle counting were used for aerosol characterization with regard to particle size and particle production quantities. Layers were characterized by scanning electron microscopy, atomic force microscopy, spectral ellipsometry, water contact angle measurements and light transmission concerning geometric properties (thickness, surface structure and roughness) and physical behaviors (i.e., optical behaviors, hydrophobicity). Results show a quasi-linear relationship of the ejection mass flow of the pneumatic-controlled atomizer and geometric layer properties which again show a direct relationship to the physical properties. No correlation was found between the aerosols before combustion and the combustion aerosols since the majority of combustion aerosol particles are synthesized solely from the gas phase based on evaporated precursor material.

ARTICLE HISTORY
Received 3 January 2020
Accepted 17 April 2020

EDITOR
Mark Swihart

1. Introduction

Combustion chemical vapor deposition (CCVD) is a cost-effective, large-scale coating method for a defined application of functional thin (nanoscaled) solid layers on substrates under atmospheric pressure. During CCVD, solid particles (i) are synthesized by flame pyrolysis of a precursor substance (gas, liquid) within an ignited combustion gas (e.g., butane-air or propane-air mixtures), (ii) are deposited on the substrate and (iii) form a disperse thin solid film. CCVD (Hunt, Carter, and Cochran 1993), which was developed primary for the purpose of adhesion promotion, is nowadays employed for applying anti-corrosion coatings, layers with increased transmission (for SiO_x) (Zunke et al. 2014), semiconducting transparent layers (based on ZnO) (Zunke et al. 2013) or for reflecting noble metal layers (Struppert et al. 2010).

Especially for thin coatings made of monodisperse silicon oxide particles (SiO_x) (Stöber, Fink, and Bohn 1968), CCVD became an established surface modification technology for various substrate materials (e.g., glass, silicon wafer, plastic) (Rüffer et al. 2013; Kretzschmar et al. 2018), whereas materials like metals, wood, stone, ceramics and textiles are also suitable. This is i. a. due to the ability of CCVD to modulate specific layer properties (e.g., layer thickness, refractive index, hydrophilicity, transmission) via the versatile combination of different CCVD process parameters (e.g., kind of precursor, substrate temperature, substrate velocity, burner-to-substrate distance).

The precursor substance as key parameter of CCVD can be supplied to the fuel gas air mixture as continuous phase (i.e., as gas or as liquid) or as disperse phase (i.e., as aerosol) by quite different methods. However, the supply of the precursor as disperse phase requires a previous aerosolization of the precursor liquid. For this purpose, different mechanisms of droplet generation were employed for CCVD in the past (Jung, Park, and Kang 2010). This includes i. a.

CONTACT Björn Sten Mark Kretzschmar bk@innovent-jena.de Innovent e.V., Prüssingstraße 27B, D-07745 Jena, Germany.

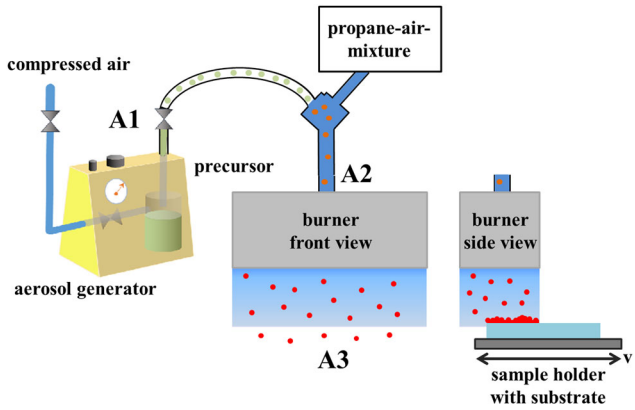

Figure 1. Schematic illustration of the operated CCVD setup; A1 = initial precursor aerosol, A2 = precursor aerosol before combustion; A3 = combustion aerosol.

ultrasonic nebulization (Cho et al. 2009; Abram et al. 2019), two-substance nozzle atomization (without coarse droplet separation) (Murakami, Yagi, and Kaneko 2005; Chang, Park, and Jang 2008) or inert gas bubble bursting (Wolden et al. 1998; Davis et al. 2004; Pfuch and Cihar 2004; Abram et al. 2019). In most studies, comprehensive analyses were performed on combustion aerosols or resulting layers, but no or less research effort was spent on the actual precursor aerosols prior combustion. Thus, there is a knowledge gap concerning the impact of precursor aerosol characteristics on layer properties. Considering the above mentioned aerosolization methods, the origin of CCVD was precursor aerosols with quite different aerosol characteristics. Ultrasonic nebulization leads typically to micrometre sized droplets in a size range between 1 – 10 µm. Two-substance nozzle atomization without coarse droplet separation is typically accompanied by droplet aerosols with bimodal size distributions, a low (<5 wt.-%) mass fraction of droplets <5 µm and a considerable mass fraction (>95 wt.-%) of droplets in the size range from 5 µm up to 200 µm.

This study focuses on the impact of precursor and combustion aerosols on layer growth, structure and properties for substrate coating by CCVD. Therefore, the objectives of this study were (i) an accurate granulometric characterization of the three relevant aerosol states (i.e., after generation, before and after combustion) for different aerosolization conditions, (ii) a multiparameter analysis of the corresponding formed layers, (iii) a comparison between the aerosol characteristics of the three states with measured layer properties and (iv) the identification of potential relationships between aerosol characteristics and layer properties.

Accomplishing these objectives was realized by the production of defined monomodal, precursor aerosols stable over time via a pneumatic-controlled two-substance atomizer (with inertia-based coarse droplet separation, also known as Collison nebulizer) was operated for precursor liquid aerosolization. Moreover, no evidence was found that such a type of atomizer was used for CCVD before. However, generated aerosols at the outlet of the atomizer as well as transformed aerosols before and after combustion were characterized granulometrically by laser diffraction spectrometry (LDS), differential electrical mobility analyses (DEMA) and condensation particle counting (CPC). Resulting solid thin layers were characterized concerning geometric properties (i.e., thickness, surface roughness) and physical behavior (reflection, hydrophobicity) by scanning electron microscopy (SEM), atomic force microscopy (AFM), spectral ellipsometry (SE), water contact angle measurements (WCA) and light transmission (UV-VIS).

2. Experimental details

2.1. Performed CCVD procedure for the preparation of thin silicon oxide films

Figure 1 provides a schematic illustration of the CCVD setup that was composed of (i) a two-substance atomizer (ATM 220 with 0.3 mm nozzle diameter, Topas GmbH, Germany) for precursor aerosol generation, (ii) a fuel-gas supply unit (50 MD-1B, SURA Instruments GmbH, Germany) to control the ratio of fuel-air mixture, (iii) a burner (Arcogas B1-100, Arcotec GmbH, Germany) for pyrolysis and (iv) a movable sample holder for substrate supply.

The two-substance atomizer as described in detail in (VDI 2017; Göhler et al. 2017) was operated in non-submerged mode with compressed air (at 1 bar, 3 bar and 5 bar system pressure) and the precursor liquid tetraethyl orthosilicate (pure TEOS, FlukaMerck, Germany). After leaving the atomizer, the generated precursor aerosols were mixed prior combustion with the fuel-gas mixture (i.e., 3.6 $L \cdot min^{-1}$ propane + 70 $L \cdot min^{-1}$ air) provided by the fuel-gas supply unit. To ensure a stoichiometric combustion, the propane to air ratio was set to 1:19.4. After ignition under these conditions, a laminar flame profile (Farris et al. 2010) with a temperature profile between 800 and 1800 °C (Burkert, Müller, and Paa 2013) is formed. Analogous to Kretzschmar et al. (2018), thin film preparation was performed on silicon wafers (p/Bor (100), single polished, Silicon Materials Inc., Germany) and float glass (4 mm, air face, Saint-Gobain Glass Deutschland GmbH, Germany) by passing the substrate with a velocity of 50 $mm \cdot s^{-1}$ for 10 times through the flame at a distance of 20 mm beneath the burner outlet.

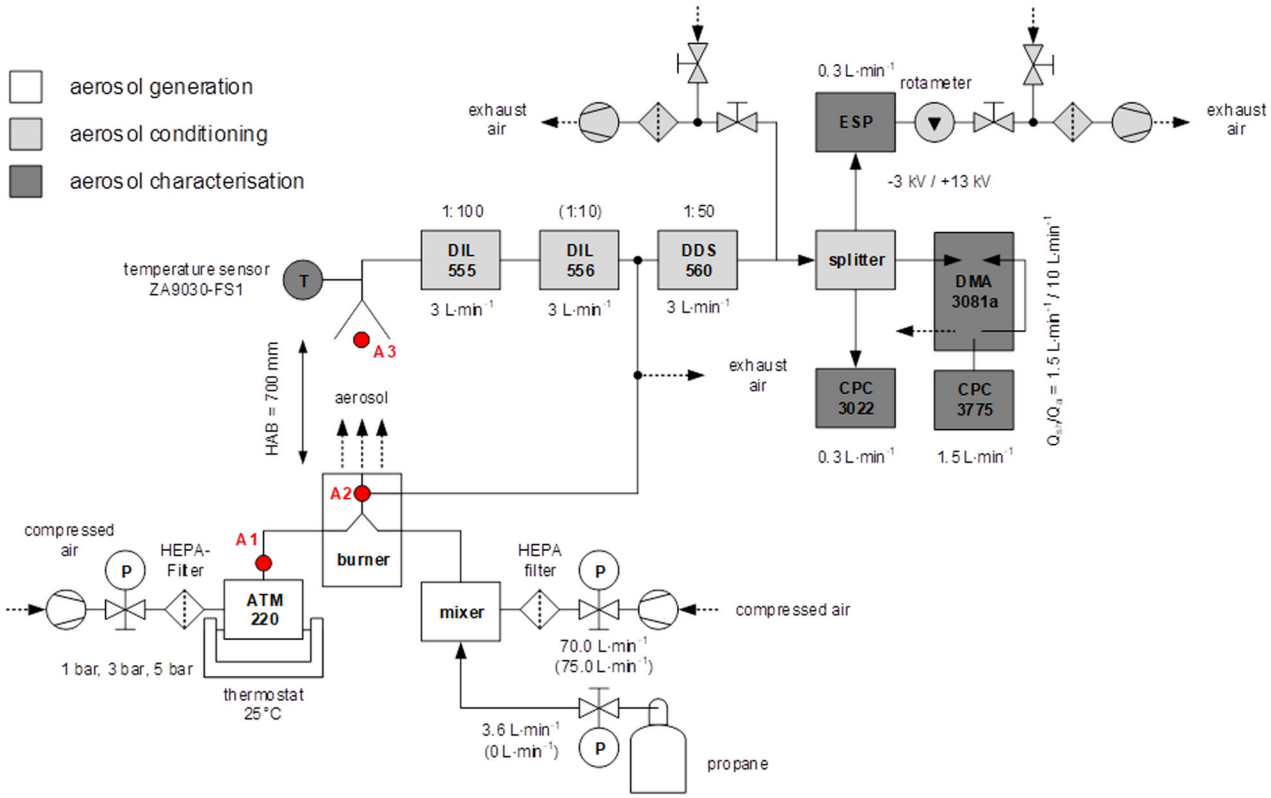

Figure 2. Schematic diagram of the experimental setup(s) operated for aerosol characterization; A1 = initial precursor aerosol at atomizer outlet; A2 = precursor aerosol immediately before combustion; A3 = combustion aerosol; ATM = two-substance atomizer; CPC = condensation particle counter; DDS = dynamic dilution system; DIL = dilution system; DMA = differential mobility analyzer; ESP = electrostatic precipitator.

2.2. Macroscopic ejection performance of the atomizer

The ejection performance (e.g., gas flow, mass flow of liquid, loading, droplet size) of atomizers depends strongly on the properties of both the propellant gas (i.e., kind of gas and quantity of flow) and the precursor liquid (i.e., density, viscosity, surface tension). Moreover, the expansion of gases (Joule and Thomson 1852), which is the basis for atomization, and droplet evaporation (May 1973) are accompanied by a temperature change that effects the liquid to be atomized due to the temperature dependency of basic liquid properties like density, viscosity and surface tension. Accordingly, preliminary analyses (designated as macroscopic analyses) were performed to characterize (i) the ejection airflow, (ii) the ejection mass flow of TEOS and (iii) the impact of cooling phenomena on the atomizer's performance.

The ejection airflow as well as the ejection mass flow were characterized for varying system pressures (i.e., operational pressure) in 0.5 bar steps from 0.5 bar up to 6.0 bar. In the case of ejection airflow analyses, the atomizer was operated without precursor liquid in combination with a precision manometer (PMM, Modell 312.20 – 6 bar, WIKA Alexander Wiegand SE & Co. KG, Deutschland). Airflows were measured by means of a bubble flow meter (BFM, Model Gilibrator 2, Sensidyne LP, USA) for volumetric airflows up to 6 L/min and a mass flow meter (MFM, Model 4040, TSI Inc., USA) for > 6 L/min. In the case of ejection mass flow analyses, an analytical balance (Kern EW 150-3 M, Components GmbH, Germany) came into operation.

To characterize the impact of cooling phenomena on the precursor liquid, the temperature change for TEOS within the liquid reservoir of the atomizer was measured for each configuration (i.e., for 1 bar, 3 bar and 5 bar system pressure) over 1 h (time resolution of 20 s) by means of a K-type thermocouple (Data-Logger Thermometer 306, Conrad Electronic SE, Germany).

2.3. Granulometric aerosol characterization

Due to the different conditions that effect the aerosol state within the CCVD setup (c.f. Figure 1), aerosol characterization was performed at three relevant regions for the three types of aerosols (A1, A2, A3), i.e., immediately at the outlet of the atomizer (A1, initial precursor aerosol, without drying effects), after

mixing with the fuel gas (A2, precursor aerosol before combustion, incl. drying effects) and after combustion (A3, combustion aerosol). For the characterization of each of the mentioned aerosols, a specific experimental setup was designed and operated. To improve the intelligibility, the three experimental setups were merged to one within Figure 2.

As mentioned above, precursor aerosol generation was realized by operating the atomizer with compressed air (system pressure of 1 bar, 3 bar, 5 bar) and the precursor liquid TEOS. To counteract precursor liquid cooling that effects considerably the ejection performance, the liquid reservoir of the atomizer was thermostated during analyses at 25 °C (Model Elmasonic P30H, Elma Schmidbauer GmbH, Germany).

At first, the initial precursor aerosol (A1) was characterized in a distance of 5 mm to the outlet of the atomizer by laser diffraction spectrometry (LDS, Model HELOS/KR-H2487, Sympatec GmbH, Germany) according to ISO (2009a). The intrinsically measured volume-weighted transformed density distributions (q_3*) based on LDS (evaluated with Fraunhofer theory, Babick 2016) covered a size range from 0.5 µm up to 175 µm (measurement range R3) and contain thus no data below 0.5 µm, but prior analyses on the base of liquids with low vapor pressure showed that an extrapolation of the whole size distribution is possible (Göhler et al. 2017). Accordingly, the received size data were fitted primary to lognormal size distributions ($q_{3,}$*) to determine the overall volume-weighted median diameter ($x_{50,3}$) and the geometric standard deviation ($\sigma_{ln,}$). Afterwards, the volume-weighted data were converted into number-weighted ones according to (Hatch and Choate 1929; ISO 2005).

Second, particle number concentrations and number-weighted particle size distributions of the precursor aerosols immediately before combustion (A2, i.e., after mixing with fuel gas, 500 mm distance from atomizer to mixing zone, 100 mm distance from mixing zone to burner) were characterized after passing a commercial bypass dilution unit (Model DDS 560, Topas GmbH, Germany) by condensation particle counting (CPC Model 3022A, TSI Inc., USA) and differential electrical mobility analysis (DEMA) according to ISO (2009b). The operated DEMA system (i.e., a scanning mobility particle sizer, SMPS Model 3938L75, TSI Inc., Shoreview, USA) that was composed of an aerosol neutralizer (Model 3077, TSI Inc., USA), a differential electrical mobility classifier (control unit Model 3082 with DMA Model 3081A, TSI Inc., USA) and a condensation particle counter (CPC, Model CPC 3775, TSI Inc., USA) was adjusted to a size range from 16 nm up to 1000 nm.

To analyze the combustion aerosols (A3), the same instruments as employed for the dried precursor aerosols prior combustion (A2) were used, but aerosol sampling as well as aerosol conditioning differed. Aerosol sampling was performed in a height above the burner of HAB = 700 mm in an open setup configuration. To avoid artifacts from background aerosols, the whole laboratory was continuously purged with particle free air by means of a laminar flow bench (Model LF-VM-K0615, STEAG Laminarflow Prozesstechnik GmbH, Germany). Additionally, two further commercial dilution units (DIL 555 and DIL 556 calibrated for 3.0 l/min, Topas GmbH, Germany) were operated for a defined reduction of the considerable high particle number concentrations. For the purpose of qualitative analyses by scanning electron microscopy (SEM, Model DSM982 Gemini, Zeiss AG, Germany), an electrostatic precipitator (ESP, prototype of Model NAS 3089, TSI Inc., USA) according to Dixkens and Fissan (1999) was operated.

The mentioned experimental conditions and setups for the granulometric characterization of the dried precursor aerosols before combustion (A2) and the ones for the combustion aerosols (A3) were prior the main analyses validated/crosschecked concerning diverse actuating variables that could have a potential effect on the results. In the case of the aerosol before combustion (A2), the particle purity of the fuel-gas mixture and the impact of the chemical composition of the process gas (i.e., fuel-gas mixture vs. particle free air) as well as the residence time within the tubing (i.e., by operation with 25 L/min, 50 L/min and 75 L/min process gas flow) were characterized. The particle number concentrations for the pure fuel-gas mixture were at least 150 times lower than the ones measured with atomizer operation (cf. Figure 6) and are thus negligible. The analyses concerning both the chemical composition and the residence time showed also no effect on the number-weighted size distributions. Accordingly, one can assume that the A2 aerosol was within the drying equilibrium. In the case of combustion aerosols (A3), the combustion of the pure fuel gas mixture and different heights above burner (i.e., 70 cm, 75 cm, 80 cm, 90 cm) were analyzed. The combustion of the pure fuel-gas mixture lead to considerable particle number concentrations up to $3{\cdot}10^{05}$ $1/cm^3$ but were more than 300 times lower than the combustion aerosols based on TEOS (cf. Figure 6). The HAB variation showed also no effects on the measured size distributions.

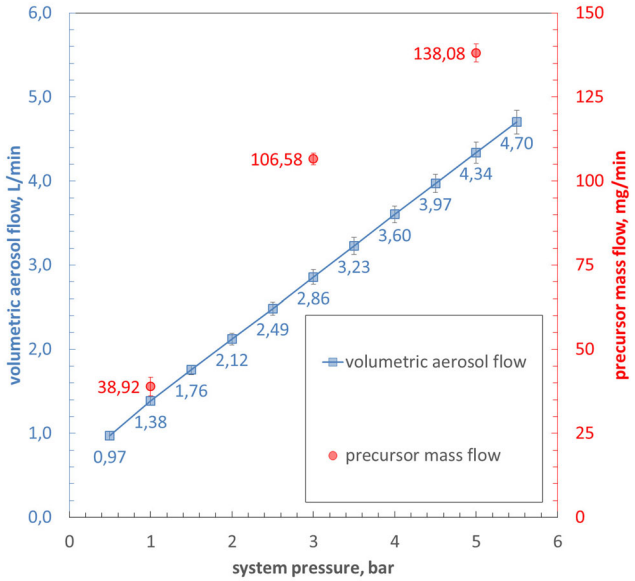

Figure 3. Ejection performance of the atomizer operated with the precursor liquid TEOS and compressed air; error bars = standard deviation (volumetric aerosol flow based on single measurements on five different nozzles identical in construction, precursor mass flow based on four measurements on one nozzle).

2.4. Layer characterization

Thin film characterization was performed concerning (i) surface structure by scanning electron microscopy (SEM), (ii) surface roughness by atomic force microscopy (AFM), (iii) layer thickness and refractive index by spectral ellipsometry (SE), (iv) hydrophobicity by water contact angle analysis (WCA) and (v) light transmission by ultraviolet/visible light (UV/VIS) spectrometry.

Surface structure or topographic analyses were performed by thermal field emission scanning electron microscopy (Model Supra 55 VP, Carl Zeiss Microscopy GmbH, Germany) with an InLens detector at 5 kV on films formed on silicon wafers.

Surface roughness characterization by AFM (Model MFP 3D Classic, Asylum Research) was performed on sample areas of (20×20) µm^2 in tapping mode with a silicon micro cantilever (Model AC160TS-R3, Olympus Corp., Japan). Received height data were used to calculate root mean square values (designated as R_q or RMS) for the description of the surface roughness according to Gadelmawla et al. (2002).

Layer thickness and refractive index were characterized by spectral ellipsometry (Model SE 850, SENTECH Instruments, Germany). Analysis were performed at 50°, 60° and 70° measuring angle, while for the purpose of data evaluation a CAUCHY model was used, with layer thickness and refractive index being the fitted parameters.

Analyses concerning the hydrophobicity of the thin films were performed by optical water contact angle analysis (Model OCA 15, DataPhysics Instruments GmbH, Germany) for layers formed on glass substrates.

Light transmission of the thin film layers on glass substrate was characterized by UV/VIS spectrometry (Model Lambda 2, PerkinElmer Inc., USA) over a wavelength range from 350 nm to 1050 nm.

3. Results and discussion

3.1. Ejection performance

Figure 3 provides at first the volumetric aerosol flow and the corresponding precursor mass flow offered by the atomizer for various system pressures.

According to Figure 3, the volumetric airflow increases linearly with the system pressure from approx. 1 L/min at 0.5 bar system pressure up to approx. 5 L/min at 6 bar system pressure. The precursor mass flow increases with increasing system pressure from 38.9 mg/min at 1 bar over 106.6 mg/min at 3 bar to 138.1 mg/min at 5 bar. The different slopes of precursor mass flow and volumetric aerosol flow are accompanied with loadings of 28.1 mg/L at 1 bar, 37.3 mg/L at 3 bar and 31.8 mg/L at 6 bar.

As mentioned before, cooling phenomena can have a significant effect on the ejection performance of the atomizer. In this context, Figure 4 shows the change of the precursor liquid temperature within the reservoir over the atomizer's operation time for different system pressures.

As it can be concluded from Figure 4, droplet drying and the Joule-Thomson effect lead for each system pressure to a significant decrease of the precursor liquid temperature over time. Moreover, one can observe that higher system pressures cause accelerated cooling and lower temperatures after 60 min. The maximum temperature decrease was determined to be approx. 2 K for 5 bar system pressure. Additional performed rheological analyses (MCR301, Anton Paar GmbH, Austria) showed that the dynamic viscosity of the used TEOS increases from (10.8 ± 2.4) mPa·s to (13.3 ± 2.4) mPa·s for a temperature decrease of 4 K from 25 °C to 21 °C. With regard to the operation times realized in this study, the viscosity change for TEOS can be neglected here. However, for the purpose of long-term operation or other precursor liquids, a thermostating of the atomizer's liquid reservoir is generally recommended.

3.2. Aerosol characteristics

Figure 5 compares the number-weighted size distributions for the analyzed system pressures of the three types of aerosol (A1, A2, A3), i.e., for the droplet size

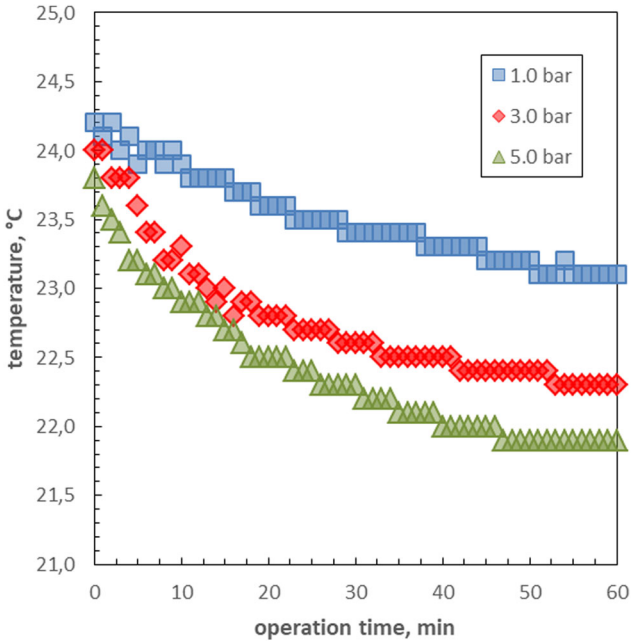

Figure 4. Influence of the Joule-Thomson effect on the precursor liquid TEOS within the liquid reservoir of the atomizer for different system pressures.

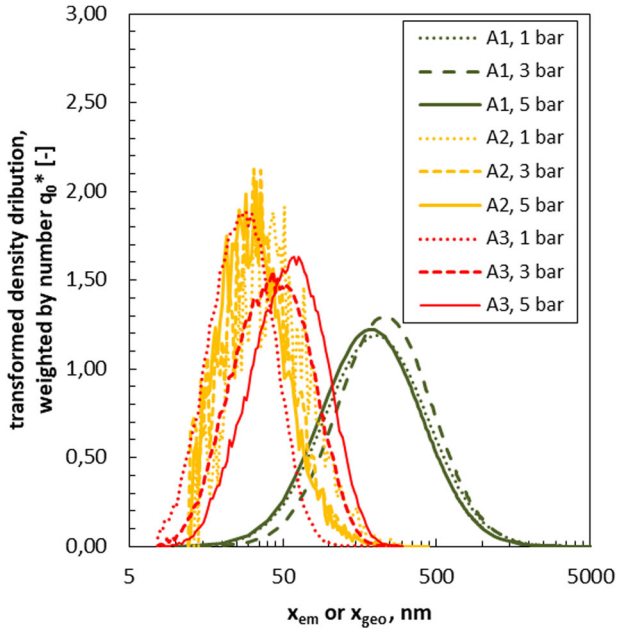

Figure 5. Mean (n = 3) number-weighted aerosol size distributions at the outlet of the atomizer (A1, based on lognormal extrapolation of LDS data), immediately prior combustion (A2, based on DEMA) and after combustion (A3, based on DEMA); x_{em} = electrical mobility diameter of DEMA, x_{geo} = projection area equivalent diameter of LDS for coarse particles and Fraunhofer theory.

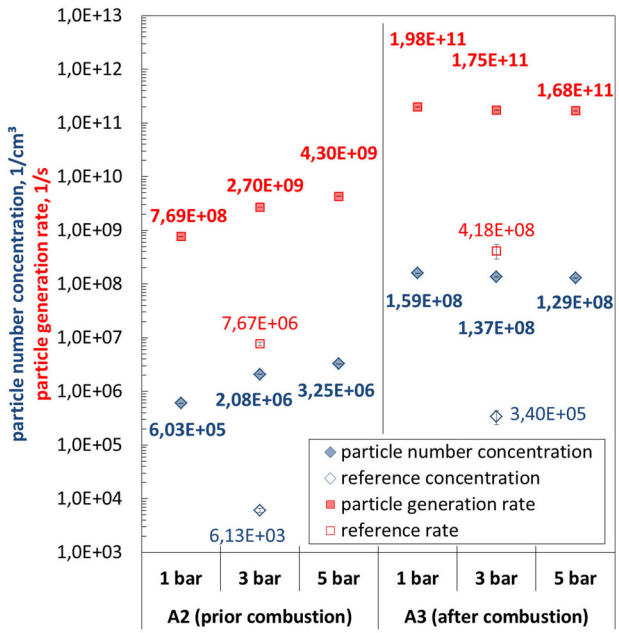

Figure 6. Mean (n = 3) particle number concentrations within the aerosol flow and calculated particle generation rates based on CNC data; reference concentrations and reference rates for A2 and A3 based on CCVD setup operation with pure fuel-mixture gas (i.e., without precursor substance TEOS).

distribution of the precursor aerosol at the outlet of the atomizer (A1), the dried precursor aerosol prior combustion (A2) and the chemical transformed combustion aerosol (A3). All size distributions are plotted over the intrinsically measured equivalent diameters, i.e., in the case of A1 over the laser diffraction equivalent diameter that corresponds here to the projection area equivalent diameter (x_{geo}) and in the cases of A2 and A3 over the electrical mobility diameter (x_{em}) that can also be seen as a kind of projection area equivalent diameter.

According to Figure 5, the system pressure shows for each type of aerosol a significant impact on the aerosol size distribution.

With increasing system pressure, the droplet size at the outlet of the atomizer (A1) decreases typically. This was also observed within the intrinsically measured volume-weighted LDS data, where the volume-weighted median diameter decreases from $x_{50,3*}$(A1, 1 bar) = 1.22 µm via $x_{50,3*}$(A1, 3 bar) = 1.04 µm to $x_{50,3*}$(A1, 5 bar) = 1.02 µm. A slight divergent behavior can be observed in Figure 5 for the number-weighted droplet size distributions, which originates from lognormal extrapolation of LDS data. Of course, the switch from 3 bar to 5 bar leads to a decrease in the number-weighted median diameter from $x_{50,0*}$(A1, 3 bar) = 231 nm to $x_{50,0*}$(A1, 5 bar) = 188 nm, but for 1 bar system pressure a number-weighted median diameter of $x_{50,0*}$(A1, 1 bar) = 203 nm results. This deviation is rather attributed to an overestimated geometric standard deviation than on the atomizer performance. Accordingly, the number-weighted droplet size distributions (A1) in Figure 5 are less suitable

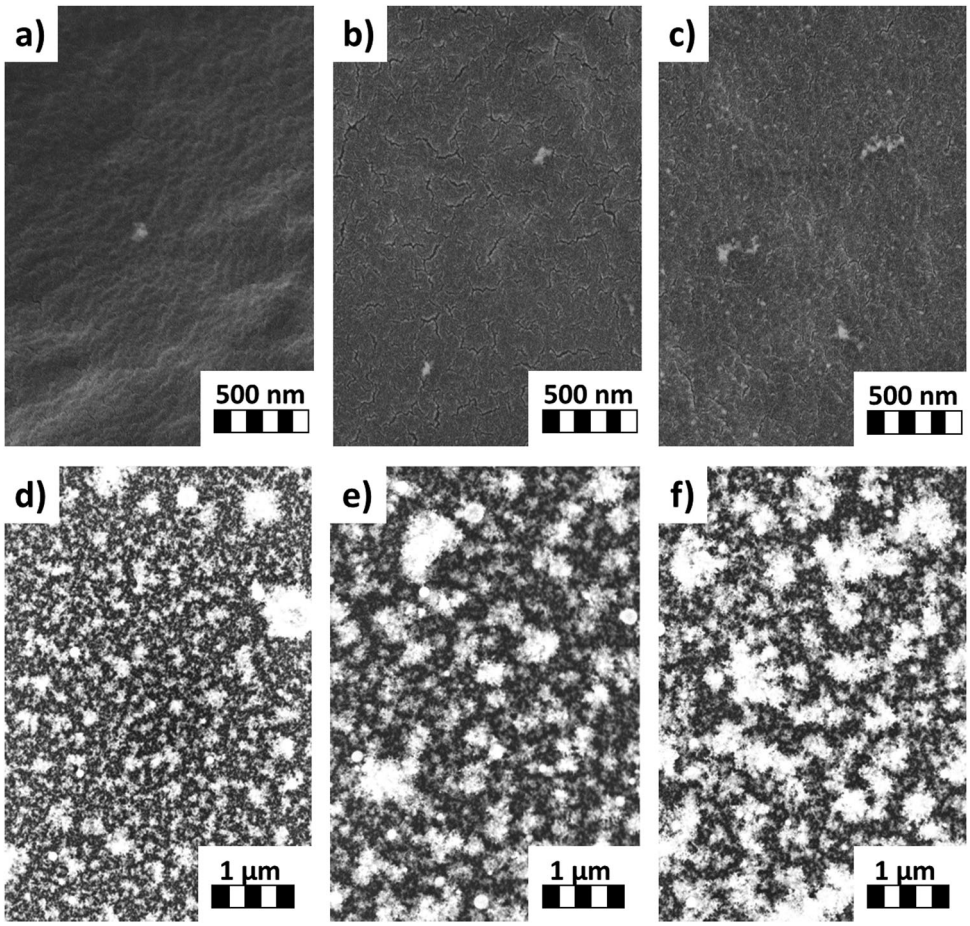

Figure 7. SEM images of electrostatically deposited combustion aerosol particles (a, b, c) and of formed films on silicon wafer (d, e, f) for 1 bar (a, d), 3 bar (b, e), and 5 bar (c, f) system pressure.

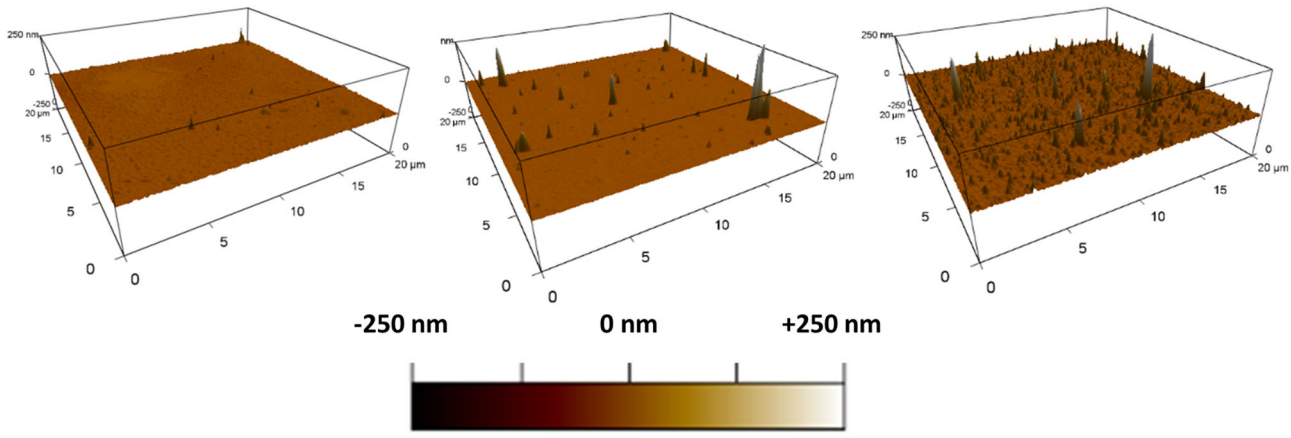

Figure 8. Surface structure by AFM analyses of the formed films on silicon wafers at 1 bar (left), 3 bar (middle) and 5 bar (right) system pressure.

for deeper discussions but allow a rough aerosol size classification in comparison to the dried aerosols before combustion and the combustion aerosols.

The dried precursor aerosol before combustion (A2) is approx. one order of magnitude finer than the droplet aerosol at the atomizer's outlet and decreases also with increasing system pressure from $x_{50,0,DEMA}$(A2, 1 bar) = 42 nm via $x_{50,0,DEMA}$(A2, 3 bar) = 34 nm to $x_{50,0,DEMA}$(A2, 5 bar) = 31 nm.

Contrary to the two above discussed correlations, the particle size of the aerosol after combustion (A3) increases with increasing system pressure from $x_{50,0,DEMA}$(A3, 1 bar) = 27 nm via $x_{50,0,DEMA}$(A3, 3 bar) = 43 nm to $x_{50,0,DEMA}$(A3, 5 bar) = 55 nm and

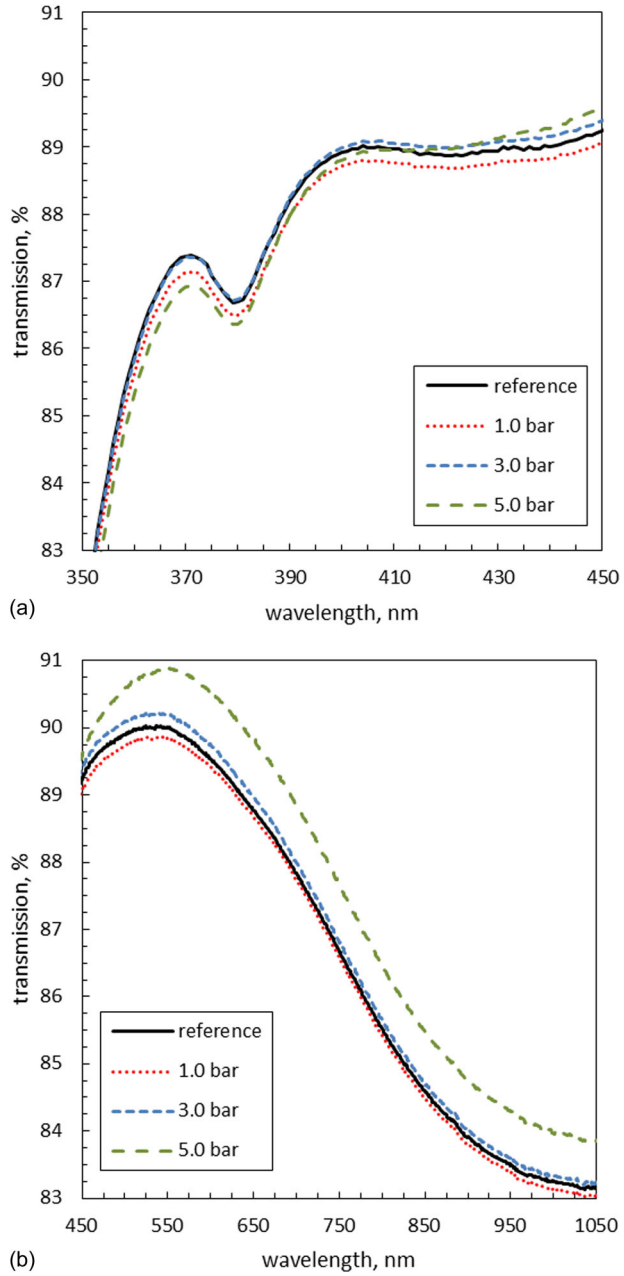

Figure 9. Transmission spectra of the formed coatings in comparison to the uncoated reference substrate.

is approx. in the same size range as the precursor aerosol before combustion (A2). In order to explain this behavior, a consideration of the prevailing particle number concentrations respectively particle generation rates of both the aerosols before combustion and after combustion is helpful (see Figure 6).

According to Figure 6, particle number concentration and particle generation rate increase with increasing system pressure for the aerosol before combustion (A2), but decrease after combustion (A3). Moreover, the total particle quantities (i.e., particle number concentration or particle generation rate) of the combustion aerosols are several times higher than for the dried precursor aerosols, i.e., 263 times at 1 bar, 66 times at 3 bar and 40 times at 5 bar.

Since also SEM images of electrostatically deposited combustion aerosol particles (see Figure 7) are in line with DEMA data and show for larger particles the typically fractal shape, the majority of combustion aerosol particles are synthesized solely from the gas phase based on evaporated TEOS. Consequently, there should be no direct correlation from the aerosols after leaving the atomizer or the dried precursor aerosol before combustion on the combustion aerosols. However, granulometric data of both types of aerosols provide clues concerning reactant impurities (here TEOS) and maybe on impurities within the layers. Consequently, separation of drying residues before combustion e.g., by filtration could be one way to improve layer impurity beside cost intensive use of ultrapure TEOS. On the other hand, condensation particle counting could be used for process monitoring for quality control.

3.3. Layer properties

Phenomenological considerations of the CCVD coatings show that the produced thin silicon oxide films were colorless and transparent on both the silicon wafers and the glass substrates.

The SEM images in Figure 7 provide a rough impression on the formed layer surface structures.

As can be deduced from the SEM images in Figure 7, the fraction of coarser aggregates/agglomerates (>0.2 µm) decreases with decreasing system pressure. Furthermore, an increasing polydispersity can be observed with increasing system pressure.

The increase of both the content of coarser agglomerates and the polydispersity is also accompanied by an increase of the surface roughness and consequently by an increase of the surface area as exemplarily shown in Figure 8 on the base of the performed AFM analyses.

AFM analysis showed for the pure reference substrate (i.e., the uncoated glass substrate) a surface roughness (i.e., root mean square) of about 0.2 nm, while for 1 bar system pressure a value of 4.7 nm was determined, followed by 9.0 nm for 3 bar and 12.5 nm for 5 bar.

However, with increasing system pressure also the refractive index increases from 1.28 for 1 bar, 1.41 for 3 bar and 1.43 for 5 bar as the SE analyses show. These values are in line with the literature (Pfuch et al. 2008) and indicate that the layers become more glass-like with increasing system pressure (theoretical refractive index of glass is 1.45). The SE analyses show furthermore an increase of the layer thickness from 39.4 nm for 1 bar via 57.6 nm for 3 bar to 93.7 nm for 5 bar.

Table 1. Determined ejection airflow, ejection precursor mass flow, median particle diameters ($x_{50,r}$) and geometric standard deviation of the particle size distributions for A1, A2, and A3 aerosols, layer thickness, refractive index, water contact angle, surface roughness, and transmission from the as-deposited silicon oxide thin layers on silicon substrate and float glass.

Property	Unit				
Aerosol generator	–	–	ATM 220	ATM 220	ATM 220
System pressure	bar	–	1	3	5
Ejection airflow	L/min	–	1.38 ± 0.05	2.86 ± 0.09	4.34 ± 0.16
Ejection precursor mass flow	mg/min		38.92 ± 2.82	106.58 ± 1.71	138.08 ± 2.67
Loading	mg/L	–	28.11	37.33	31.84
$x_{50,3*}$ (A1)	µm	–	1.22	1.04	1.02
Geometric standard deviation	–	–	2.17	2.03	2.12
$x_{50,0,DEMA}$ (A2)	nm		41.9 ± 1.8	33.7 ± 0.6	31.4 ± 0.5
Geometric standard deviation	–		1.74	1.67	1.63
Particle generation rate (relative standard deviation)	1/s		0.77 × 1009 (±0.74%)	2.70 × 1009 (±0.76%)	4.30 × 1009 (±0.70%)
$x_{50,0,DEMA}$ (A3)	nm		26.9 ± 0.6	42.6 ± 0.5	54.7 ± 0.8
Geometric standard deviation	–		1.59	1.75	1.73
Particle generation rate (relative standard deviation)	1/s		1.98 × 1011 (±1.76%)	1.75 × 1011 (±1.89%)	1.68 × 1011 (±1.98%)
Surface roughness R_q	nm	0.2[a]	4.7	9.0	12.5
Layer thickness d	nm	–	39.4 ± 1.2	57.6 ± 1.5	93.7 ± 2.1
Refractive index n_{Layer}	–	–	1.28 ± 0.02	1.41 ± 0.01	1.43 ± 0.01
Water contact angle Θ	°	20.0[a]	31.6	21.7	<5[b]
Transmission T @ 550 nm	%	90.0[a]	89.8	90.2	90.9

[a]Untreated reference substrate.
[b]Below detection limit.

WCA analyses show, that the water contact angle of the layers decreases from 31.6° (1 bar) via 21.7° (3 bar) to <5° (below detection limit, bar) with increasing system pressure. Accordingly, the layers become increasingly hydrophilic. This correlates well with the increase of the surface area that is accompanied with a higher area-specific number of OH groups and thus with a higher surface energy.

As already indicated by the changes in the refractive index, the optical properties of the formed layers changes significantly. Figure 9 shows therefore the transmission spectra of the formed layers in comparison to the one received for the non-coated reference glass substrate. To improve the visualization of changes below 450 nm, the whole transmission spectrum is shown over two diagrams with different scaling.

As it can be deduced from Figure 9, the transmission spectra of the formed layers differ from the spectrum of the non-coated reference substrate. The layer formed at 5 bar, showed at a wavelength of 550 nm with 90.9% the highest transmittance, followed by the 3 bar layer with 90.2% and the 1 bar layer with 89.8%. This is due to two effects that significantly influence the transmission. An increase in layer thickness up to a maximum of 140 nm leads to an increased transmission. At the same time, a higher refractive index leads to lower transmission. The transmission improvement of samples with low refractive index is up to 2%, while this of higher refractive index is 1%. In contrast, the transmission improvement of layer thicknesses in the range of 40 nm is 0.5% and at 100 nm 2% (Pfuch et al. 2008). In combination of a low refractive index and a low layer thickness (1 bar), the transmission improvement is low (in this case negative). There is a transmission improvement for a high refractive index and a high layer thickness (5 bar) of about 1%. In comparison to the literature (Raut et al. 2013), this is a slight improvement.

3.4. Comparison of aerosol characteristics and layer properties

The most relevant data on the ejection performance of the atomizer, the aerosol characteristics and the corresponding layer properties are summarized in Table 1.

Table 1 shows a linear relationship between system pressure of the nebulizer and the aerosol properties. It also shows a linear relationship with the layer properties. An increase in the system pressure results in an increase of ejection air flow as well as the ejection mass flow and the particle generation rate (before and after combustion). In addition, an increase in the system pressure leads to an increase in the layer thickness, the surface roughness (and thus the surface area) and the refractive index.

4. Summary and conclusion

To characterize the modulation of silica layer properties by varying the granulometric state of tetraethyl orthosilicate precursor aerosols during CCVD, a commercial two-substance atomizer (with inertia-based coarse droplet separation) was operated for precursor liquid aerosolization. In a comprehensive testing program, both aerosol characteristics and layer properties were analyzed. Aerosol characterization was performed on the initial generated aerosols at the atomizer's outlet (A1) by

LDS and on the transformed aerosols immediately before (A2) and after combustion (A3) by DEMA and CNC. Formed layers were characterized concerning geometric properties (i.e., thickness, surface roughness) and physical behavior (reflection, hydrophobicity, transmittance) by SEM, AFM, SE, WCA and UV-VIS).

The analyses showed in most cases a quasi-linear relationship between system pressure of the pneumatic-controlled atomizer and aerosol characteristics as well as layer properties. Thus, an increase of the system pressure was accompanied with an increase of ejection airflow, ejection mass flow, particle generation rate (before and after combustion), layer thickness, surface roughness (and thus surface area) and refractive index. Contemporaneously, the water contact angle of the layers decreases with increasing system pressure, i.e., the layers become increasingly hydrophilic that is attributed to surface-specific number of OH groups.

No correlation was found between the aerosol states before combustion (i.e., for the droplet size at the atomizer's outlet and the dried aerosol before combustion) and the combustion aerosols. This is caused by the fact that the majority of combustion aerosol particles are synthesized solely from the gas phase based on evaporated TEOS. But granulometric data of aerosols before combustion provide clues concerning reactant impurities and maybe on impurities within the layers. Consequently, separation of drying residues before combustion e.g., by filtration could be one way to improve layer impurity beside cost intensive use of ultrapure TEOS. On the other hand, condensation particle counting could be used for process monitoring for quality control.

Conflict of interests

The authors declare no conflict of interest.

Authors' contributions

All authors discussed the initial outline of the manuscript. B. Kretzschmar (Innovent) performed CCVD and thin film characterization, data evaluation, data interpretation, drafting and critical revision of the manuscript. P. Bergelt (TUD) performed aerosol analysis, data evaluation, data interpretation, drafting and critical revision of the manuscript. D. Göhler (TUD, Topas) performed experimental study design for aerosol analysis, data evaluation, data interpretation, drafting and critical revision of the manuscript. F. Firmbach (Innovent) performed data evaluation, data interpretation, drafting and critical revision of the manuscript. R. Köcher (Innovent), A. Heft (Innovent), M. Stintz (TUD) and B. Grünler (Innovent) supervised the study, performed data interpretation, and revised critically the manuscript according to their field of research.

Endnotes

The graphical representation, the used symbols as well as the vocabulary to describe particle size distributions, are in line with ISO (1998) and ISO (2013). In the case of transformed size distributions, the logarithm to the base of 10 was operated instead of the natural logarithm.

Abbreviations

AFM	atomic force microscopy
ATM	atomizer
BFM	bubble flow meter
CCVD	combustion chemical vapor deposition
CPC	condensation particle counter
DDS	dynamic dilution system
DEMA	differential electrical mobility analysis
DIL	dilution system
DMA	differential mobility analyzer
ESP	electrostatic precipitator
HEPA	filter, high efficiency particulate air filter
LDS	laser diffraction spectrometry
MFM	mass flow meter
SEM	scanning electron microscopy
SMPS	scanning mobility particle sizer
TEOS	tetraethyl orthosilicate
UV	ultraviolet light
VIS	visible light
WCA	water contact angle analysis

Funding

This work was supported by the German Federal Ministry for Economic Affairs and Energy (BMWI) via the project supporter EuroNorm under grand MF160129.

ORCID

Fabian Firmbach http://orcid.org/0000-0003-0769-9187

References

Abram, C., M. Mezhericher, F. Beyrau, H. A. Stone, and Y. Ju. 2019. Flame synthesis of nanophosphors using submicron aerosols. *Proc. Combust. Inst.* 37 (1):1231–9. doi: 10.1016/j.proci.2018.06.040.

Babick, F. 2016. Fraunhofer diffraction. In *Suspensions of colloidal particles and aggregates*, ed. F. Babick, 318. 1st ed. Heidelberg: Springer. doi:10.1007/978-3-319-30663-6.

Burkert, A., D. Müller, and W. Paa. 2013. Si and SiO detection in a HMDSO/propane/air flame using spatially resolved optical emission spectroscopy (OES). *J. Quant. Spectrosc. Radiat. Transf.* 114:101–8. doi:10.1016/j.jqsrt.2012.08.020.

Chang, H., J.-H. Park, and H. D. Jang. 2008. Flame synthesis of silica nanoparticles by adopting two-fluid nozzle

spray. *Colloids Surf. A* 313-314:140–4. doi:10.1016/j.colsurfa.2007.04.083.

Cho, K., H. Chang, D. S. Kil, J. Park, H. D. Jang, and H. Y. Sohn. 2009. Mechanisms of the formation of silica particles from precursors with different volatilities by flame spray pyrolysis. *Aerosol Sci. Technol.* 43 (9):911–20. doi:10.1080/02786820903025986.

Davis, M., G. Benito, D. Sheel, and M. Pemble. 2004. Growth of thin films of molybdenum and tungsten oxides by combustion CVD using aqueous precursor solutions. *Chem. Vap. Depos.* 10 (1):29–34. doi:10.1002/cvde.200306260.

Dixkens, J., and H. Fissan. 1999. Development of an electrostatic precipitator for off-line particle analysis. *Aerosol Sci. Technol.* 30 (5):438–53. doi:10.1080/027868299304480.

Farris, S., S. Pozzoli, P. Biagioni, L. Duó, S. Mancinelli, and L. Piergiovanni. 2010. The fundamentals of flame treatment for the surface activation of polyolefin polymers – A review. *Polymer* 51 (16):3591–605. doi:10.1016/j.polymer.2010.05.036.

Gadelmawla, E. S., M. M. Koura, T. M. A. Maksoud, I. M. Elewa, and H. H. Soliman. 2002. Roughness parameters. *J. Mater. Process. Technol.* 123 (1):133–45. doi:10.1016/S0924-0136(02)00060-2.

Göhler, D., S. Große, A. Bellendorf, T. A. Falkenstein, M. Ouaissi, J. Zieren, M. Stintz, and U. Giger-Pabst. 2017. Hyperthermic intracavitary nano-aerosol therapy (HINAT) as improved approach for pressurised intraperitoneal aerosol chemotherapy (PIPAC): Technical description, experimental validation and first proof of concept. *Beilstein J. Nanotechnol.* 8:2729–40. doi:10.3762/bjnano.8.272.

Hatch, T., and S. P. Choate. 1929. Statistical description of the size properties of non uniform particulate substances. *J. Franklin Inst.* 207 (3):369–87. doi:10.1016/S0016-0032(29)91451-4.

Hunt, A. T., W. B. Carter, and J. K. Cochran. 1993. Combustion chemical vapor deposition: A novel thin-film deposition technique. *Appl. Phys. Lett.* 63 (2):266–8. doi:10.1063/1.110362.

ISO (International Organization for Standardization). 1998. *ISO 9276-1:1998. Representation of results of particle size analysis – Part 1. Graphical representation*. Genva, Switzerland.

ISO. 2005. *ISO 9276-5:2005. Representation of results of particle size analysis - Part 5. Methods of calculation relating to particle size analyses using logarithmic normal probability distribution*. Genva, Switzerland.

ISO. 2009a. *ISO 13320:2009. Particle size analysis – Laser diffraction methods. Genva, Switzerland.*

ISO. 2009b. *ISO 15900:2009. Determination of particle size distribution - Differential electrical mobility analysis for aerosol particles*. Genva, Switzerland.

ISO. 2013. *ISO 26824:2013. Particle characterization of particulate systems - vocabulary*. Genva, Switzerland.

Joule, J., and W. Thomson. 1852. On the thermal effects experienced by air in rushing through small apertures. *Lond. Edinb. Dublin Philos. Mag. J. Sci.* 4 (28):481–92. doi:10.1080/14786445208647169.

Jung, D. S., S. B. Park, and Y. C. Kang. 2010. Design of particles by spray pyrolysis and recent progress in its application. *Korean J. Chem. Eng.* 27 (6):1621–45. doi:10.1007/s11814-010-0402-5.

Kretzschmar, B., K. Assim, A. Preuß, A. Heft, M. Korb, M. Pügner, T. Lampke, B. Grünler, and H. Lang. 2018. Cobalt and manganese carboxylates for metal oxide thin film deposition by applying the atmospheric pressure combustion chemical vapour deposition process. *RSC Adv.* 8 (28):15632–40. doi:10.1039/C8RA02288G.

May, K. 1973. The collison nebulizer: Description, performance and application. *J. Aerosol Sci.* 4 (3):235–43. doi:10.1016/0021-8502(73)90006-2.

Murakami, K., I. Yagi, and S. Kaneko. 2005. Oriented growth of tin oxide thin films on glass substrates by spray pyrolysis of organotin compounds. *Journal of the American Ceramic Society* 79 (10):2557–62. doi:10.1111/j.1151-2916.1996.tb09015.x.

Pfuch, A., and R. Cihar. 2004. Deposition of SiOx thin films by microwave induced plasma CVD at atmospheric pressure. *Surf. Coat. Technol.* 183 (2-3):134–40. doi:10.1016/j.surfcoat.2003.09.052.

Pfuch, A., T. Tölke, A. Heft, T. Richter, A. Niemann, A. Rechtenbach, and O. Frigge. 2008. Glass covers for photovoltaic applications with enhanced transmission and self-cleaning properties. In *Solar energy: Research, technology and applications*, ed. W. L. Olofsson and V. I. Bengtsson, 317–47. 1st ed. New York: Nova Science Publishers.

Raut, H. K., A. S. Nair, S. S. Dinachali, V. A. Ganesh, T. M. Walsh, and S. Ramakrishna. 2013. Porous SiO2 anti-reflective coatings on large-area substrates by electrospinning and their application to solar modules. *Sol. Energy Mater. Sol. Cells* 111:9–15. doi:10.1016/j.solmat.2012.12.023.

Rüffer, P., A. Heft, R. Linke, T. Struppert, and B. Grünler. 2013. Characterisation of thin SiOx-layers on float glass deposited by combustion chemical vapour deposition (C-CVD). *Surf. Coat. Technol.* 232:582–6. doi:10.1016/j.surfcoat.2013.06.031.

Stöber, W., A. Fink, and E. Bohn. 1968. Controlled growth of monodisperse silica spheres in the micron size range. *J. Colloid Interface Sci.* 26 (1):62–9. doi:10.1016/0021-9797(68)90272-5.

Struppert, T., A. Jakob, A. Heft, B. Grünler, and H. Lang. 2010. The use of silver(I)-2-[2-(2-methoxyethoxy)ethoxy]acetate as precursor in the deposition of thin silver layers on float glass by the atmospheric pressure combustion chemical vapor deposition process. *Thin Solid Films* 518 (20):5741–4. doi:10.1016/j.tsf.2010.05.082.

VDI (Association of German Engineers). 2017. *VDI 3491-2: 2017. Measurement of particles – Methods for generating test aerosols – Part 2: Dispersing liquids*. Berlin, Germany.

Wolden, C., R. Davis, Z. Sitar, and J. Prater. 1998. Flat-flame diamond CVD: The effect of pressure and operating conditions for specific applications. *Diamond Relat. Mater.* 7 (2-5):133–8. doi:10.1016/S0925-9635(97)00206-9.

Zunke, I., A. Heft, P. Schäfer, F. Haidu, D. Lehmann, B. Grünler, A. Schimanski, and D. Zahn. 2013. Conductive zinc oxide thin film coatings by combustion chemical vapour deposition at atmospheric pressure. *Thin Solid Films* 532:50–5. doi:10.1016/j.tsf.2012.11.151.

Zunke, I., P. Rüffer, T. Tölke, A. Heft, B. Grünler, and A. Schimanski. 2014. Deposition of thin functional coatings at atmospheric pressure using combustion chemical vapour deposition. In *Combustion: Types of reactions, fundamental processes and advanced technologies*, ed. J. M. Grier, 121–68. 1st ed. New York: Nova Science Publishers.